Estimating leaf and canopy nitrogen contents in major field crops across the growing season from hyperspectral images using nonparametric regression

Dong wang[1]

[1]Affiliation not available

November 27, 2023

Dong Wang[a,b], Paul C. Struik[a], Lei Liang[b,*] & Xinyou Yin[a,*]

[a] Centre for Crop Systems Analysis, Department of Plant Sciences, Wageningen University & Research, P.O. Box 430, 6700 AK Wageningen, The Netherlands

[b] Shanghai Lankuaikei Technology Development Co. Ltd., No. 888 Huanhu West 2nd Road, Pudong New District, Shanghai, China

[*]Corresponding Authors

E-mail address: xinyou.yin@wur.nl, lei.liang@lankuaikei.cn

Abstract

Estimating leaf nitrogen (N) status is crucial for site- and time-specific crop N management, and can be accomplished more routinely than ever before with the advent of hyperspectral imaging techniques. We conducted field experiments with different nitrogen supply for rice, wheat and maize, in China, in which three types of hyperspectral features were extracted, including canopy reflectance (Ref), vegetation indices (VIs), and texture information (Tex). These features as well as crop development stage (DS) were applied to estimate crop N parameters, using five nonparametric regression algorithms: Partial Least Squares Regression (PLSR), Support Vector Regression (SVR), Random Forest Regression, Deep Neural Network, and Convolution Neural Network. The performance of PLSR and SVR models was more robust than that of the others and could be improved by incorporating the combined feature set RefVIsTex, although there was no further improvement when also incorporating DS. The prediction of the mass-based leaf N trait, leaf N concentration (LNC), was better than that of the area-based trait, specific leaf N (SLN). The models also predicted specific leaf area (SLA) better than its reciprocal, specific leaf weight. Values of SLN were better predicted via an indirect method (predicted via SLA; denoted as SLN_{sla}) than via the direct method (SLN_{dir}). However, when upscaled to canopy, the predicted canopy N content (N_{canopy}) using SLN_{dir} agreed better with measured N_{canopy} than that using SLN_{sla}, and even better than the direct prediction $N_{canopy,dir}$ in rice and maize. These results were discussed in view of coupling the predicted leaf and canopy N traits with dynamic crop growth models that can be used for optimizing field N management in sustainable agricultural production.

Keywords

Major crop, nonparametric regression algorithm, hyperspectral image, leaf nitrogen trait, crop nitrogen management

1. Introduction

The security and sustainability of modern agricultural production are at risk. While crop production has increased 50% since 2000, global agricultural land area decreased by 2% and the overall fertilizer use was 40% higher in 2018 than in 2000, while 52% of the increase was nitrogen (N) (FAO, 2020). Fertilization with N is needed as it strongly influences crop growth, production and quality (Beeckman et al., 2018; Lemaire et al., 2008) while soils often cannot supply enough N to meet the demands of modern varieties to achieve high yields. Crop N uptake, the N absorption by the roots, depends on soil N availability and crop N demand. Crop demand changes during the vegetative and reproductive phases, while N movement and reallocating within the crop occur as well (Ohyama, 2010). Based on the understanding of these and other physiological processes, numerous dynamic crop models have been developed (e.g., Kropff et al., 1994; Yin and Struik, 2017), which can simulate responses of crop growth to N fertilization. In general, N fertilization can increase crop yield. However, in view of the cost of N fertilizers and the diminishing return of productivity (yield gain per unit N-fertilizer diminishes with increasing application of N), the amount of fertilizers applied to crops may be excessive (Schröder et al., 2000; Skiba, 2014). Moreover, severe environmental issues have arisen because of N losses, through volatilization (Davidson, 2009), leaching (Padilla et al., 2018) and runoff (Zeng et al., 2021). Thus, it is necessary to guide farmers to perform a sustainable site- and time-specific N-fertilizer management (Weiss et al., 2020). To this end, monitoring crop N status in time and linking this with crop models to more accurately predict crop growth (Jin et al., 2018) may allow the development of effective strategies for smart crop N management.

Monitoring crop N status via destructive sampling and biophysical chemical analyses of crop N is costly and time consuming. Instead, remote sensing has been developed as a powerful tool to monitor crop N status. Although multispectral satellite images tend to be temporally frequent, hyperspectral satellite images suit better for crop phenotyping because of the higher spectral resolution (Marshall and Thenkabail, 2015). However, hyperspectral satellite images cannot be acquired in time: delivery always takes weeks, while crop N status rapidly changes especially during the vegetative phase, like from tillering to panicle-initiation for rice, during which fertilizers are applied mostly. Consequently, hyperspectral sensors equipped on an Unmanned Aerial Vehicle (UAV) serve with a high versatility for meeting the requirements on spectral, spatial, and temporal resolution (Homolová et al., 2013). Of the studies on predicting N from hyperspectral images in an agricultural context, more than two thirds are about rice, wheat and maize (Berger et al., 2020), mirroring the large agricultural areas around the globe cropped with these crops (Khoury et al., 2014).

For site-specific field N management, the monitoring of the aboveground leaf-N content in a canopy (N_{canopy}) is crucial as it determines canopy photosynthetic capacity and thus crop productivity (Peng et al., 1995). In crop models, canopy photosynthesis is calculated as the integration of photosynthetic rates of individual leaves in a canopy, while leaf photosynthesis is often related to leaf N status (Boote et al., 1998; Kropff et al., 1994; Yin & van Laar 2005). To parameterize this relationship, data for leaf photosynthesis as measured by gas exchange are used, which are expressed on a leaf-area basis (Evans, 1983). It follows that leaf-N parameters used to model leaf photosynthesis are also expressed on a leaf area basis. Indeed, specific leaf N content (SLN, g N m^{-2}) has been widely used as a typical leaf-N parameter in crop models to calculate leaf photosynthesis rate (Evans, 1983; Kropff et al., 1994; Wang et al., 2022; Yin et al., 2009). Thus, predicting crop N status (e.g., based on SLN) from UAV-based hyperspectral imaging and linking this prediction with crop modelling can guide farmers for better crop N management.

Investigating SLN is also supported by the expectation that the light reflected or transmitted by a leaf is considered to interact within the whole leaf thickness in spectral domains of absorption, and thus, the reflectance and transmittance are supposed to be more directly sensitive to the variation in the area-based content of absorbing constituents, like SLN, but rather less to the mass-based concentration, leaf N concentration (LNC, g g^{-1}) (Baret and Fourty, 1997). However, it is surprising that the estimation of SLN is still rare (Berger et al., 2020) whereas there are many studies regarding the prediction of LNC from remote sensing images (e.g., Moharana and Dutta (2016); Raj et al. (2021)). Very few studies have compared predictions of SLN and LNC. For instance, Ecarnot et al. (2013) showed that the prediction of LNC in wheat leaf samples collected from a broad range of genotypes (wild and cultivated forms) had better accuracy than that of SLN. However, Li et al. (2018) found that SLN in rice and wheat had better correlation than LNC with the determined

features in the shortwave infrared region (1000 to 2500 nm). Given that these few studies already showed inconsistencies, predictions of SLN and LNC should be further evaluated and compared, especially across various crop species.

On the other hand, SLN can be calculated from LNC, using the leaf thickness parameter specific leaf weight (SLW, g m^{-2}) (Baret and Fourty, 1997), or its reciprocal, specific leaf area (SLA, m^2 g^{-1}). This implies that, while SLN can be directly predicted, it can also be indirectly estimated based on the prediction of LNC and SLW or SLA. Note that SLA is a parameter that can inherently cause differences in photosynthetic N use efficiency across species (Poorter and Evans, 1998); therefore, predicting SLA may generate additional information. While it has been reported that SLN in wheat was better predicted by the indirect approach than by the direct method (Ecarnot et al., 2013), a comparison of performance of indirect and direct approaches in predicting SLN is yet to be made for more species. Similarly, the performance of indirectly predicted N_{canopy} by upscaling SLN and LNC, compared with that of the directly predicted N_{canopy}, should be investigated as well. Kattenborn et al. (2019) indicated that the area-based indicators of leaf pigment are supposed to be more suitable for upscaling from leaf to canopy level, since upscaling area-based leaf N only requires an estimate of the canopy state variable leaf area index (LAI), as is done in crop models (Kropff et al., 1994; Yin and Struik, 2017). Nevertheless, the prediction of area- and mass-based leaf N for upscaling from leaf to canopy level need to be further quantified.

Methodologies relating to N prediction from remote sensing have been developed since the pioneering work by Thomas and Oerther (1972). Generally, predicting methods can be classified into four categories: parametric regression methods like methods based on vegetation indices (VIs), nonparametric regression methods including linear and nonlinear regression algorithms, physical methods like inversion of radiative transfer models, and hybrid regression methods by combining physically based methods with nonparametric regression methods (Verrelst et al., 2019). Nonparametric regression methods, which explore the direct link between target traits and the given spectral data, are receiving more attention than the other three methods in the recent decade (Berger et al., 2020). Although regression algorithms like Artificial Neural Networks (ANN) have been employed in recent studies (Liu et al., 2016; Yao et al., 2015), deep learning (DL)-based regression methods, such as Deep Neural Network (DNN) and Convolution Neural Network (CNN), are still under-utilized for crop N prediction based on canopy-level hyperspectral reflectance (Fu et al., 2020). Given that DNN has shown more potential than other regression methods in combining different types of features, like canopy spectral, VIs and texture information, for predicting soybean yield (Maimaitijiang et al., 2020), predicting leaf and canopy N by DL-based regression algorithms should be explored.

Spectral and textural features are fundamental pattern elements in imagery interpretation. The full spectrum has been widely used in chemometrics (Atzberger et al., 2010), while the spectrum within visible (VIS, 400 to 700 nm) and near infrared (NIR, 800 to 1300 nm) regions are frequently reported for crop N estimation (Homolova et al., 2013). For instance, as a chlorophyll molecule contains four N atoms, there is an association between N supply and reflectance of the visible (400 to 700 nm) spectrum and also the so-called red-edge, located between VIS and NIR and defined as the position of the sharp change in leaf reflectance between 680 to 750 nm (e.g. Horler et al., 1983; Berger et al., 2020). Serbin et al. (2012) suggested that visible and NIR spectra data could be promising raw data to establish the robust calibration that allows to infer some leaf parameters such as LNC and its temporal variation. Spectral information has also been widely used in numerous VIs. While spectral features describe the variations in various bands of an electromagnetic spectrum, textural features contain the information about the spatial characteristics of canopy architecture within a band (Colombo, 2003; Haralick et al., 1973). Fusing canopy texture information together with spectral features is gaining momentum in phenotyping crop traits such as LAI (Liu et al., 2021), biomass (Zheng et al., 2018b), and yield (Maimaitijiang et al., 2020). Zheng et al. (2018a) showed that LNC in rice was better predicted after incorporating texture information into VIs by using stepwise multiple linear regression. Thus, texture features should also be taken into consideration in predicting SLN and N_{canopy}. Especially, taking advantage of high spatial resolution of the UAV-acquired hyperspectral images (the ground pixel size is usually less than a meter), texture information is supposed to be one type of the important features in site-specific field N management.

In this study, the prediction of area- and mass-based leaf N traits from hyperspectral images will be conducted by combining canopy spectral, VIs and texture information by nonparametric regression algorithms for three major crops (rice, wheat, maize). Our objectives are: 1) to explore the utilization of the combinations of different feature types and nonparametric regression algorithms in the prediction of leaf N traits at leaf level, SLN and LNC, and at canopy level, N_{canopy}, in different crop species; 2) to compare the performance in estimating N_{canopy} between directly predicted N_{canopy} and its values upscaled from SLN and LNC; and 3) to identify the most robust nonparametric regression algorithms and the most effective pathways (direct vs. indirect) that can be applied in obtaining crop N information of major crops. Achieving these objectives would help monitor crop N status that can be linked with crop models for more accurately predicting crop growth and guide N-fertilizer management in the context of sustainable precision agriculture.

2. Materials & Methods

2.1 Experimental design

Field experiments with different N rates from deficient to excessive were conducted in China: rice experiment was in Chongming, Shanghai, while maize and winter wheat experiments were in Luohe and Zhoukou, respectively, Henan province (Fig. 1). Treatments for each experiment were arranged as a randomized block design. There were four replications (four blocks) in the rice experiment, and within each block, six N rates, varying from 0 to 320 kg N ha^{-1}, were applied to rice (cv. Nanjing 46), planted on 4 June 2020 with a row spacing of 20 cm and a within-row plant spacing of 2-3 cm. The plot size was 6 x 30 m. Experiments of maize (cv. Zhengdan 958) and winter wheat (cv. Bainong 4199) were designed with eight blocks, and in each block seven N rates, varying from 0 to 400 kg N ha^{-1}, were applied. Each plot of maize was 10 x 20 m and each plot of wheat was 9 x 18 m (Fig. 1). Maize was sown on 9 June 2020 with 60 cm row spacing and 25 cm plant spacing in the row. Winter wheat was planted after harvesting maize on 24 October 2020 with a row spacing of 21 cm and a within-row plant spacing of 1-2 cm. Urea N fertilizer (N, 46%) was split-applied according to the rate and the time schedule described in Table S1. Based on the local practice, for each experiment, sufficient phosphate (112.5, 120 and 75 kg $P_2O_5ha^{-1}$ for rice, maize and winter wheat, respectively) and potash (112.5, 120 and 105 kg K_2O ha^{-1} for rice, maize and winter wheat) fertilizers were applied to prevent phosphorus and potassium deficiencies. Irrigation, and pest, disease and weed control were the same for all treatments within a crop species and followed local standard practices. Figure 2 presents a flow chart detailing the overall procedure used in this study. The acronyms of the targeted leaf traits at the leaf and canopy level are summarized in Table 1.

2.2 Data acquisition

2.2.1 Canopy leaf trait measurements

Crops were destructively sampled from all experimental plots on six dates (Table 2). At each sampling date, aboveground plants were cut within an area of 2.25, 2.4, and 1.0 m^2 in each plot for rice, wheat and maize, respectively. The total fresh samples were weighted immediately and ca. 20% of the biomass was used as subsamples to be dissected into component plant parts, including green leaves, stems, and grains. Yellow leaves were not included. LAI was measured on the fresh green leaves using a LI-3100C Area Meter (Li-Cor, Lincoln, NE, USA). Then, green leaves were weighed after being oven-dried at 70°C to constant weight. All green leaf samples were mixed and ground, and then stored for chemical testing. LNC, expressed on the basis of leaf dry weight, was determined by the Micro-Keldjahl method. N_{canopy} was calculated as the product of LNC and leaf weight per unit ground area. SLW was calculated as the ratio of leaf weight to LAI and SLA was calculated as 1/SLW. SLN was calculated as the product of LNC and SLW. Data records of wheat at maturity were excluded in this study, as there were no green leaves remaining at that time.

2.2.2 Canopy reflectance measurements

Canopy reflectance data were obtained before each field destructive sampling by a Cubert S185 hyperspectral snapshot camera (Cubert GmbH, Ulm, Baden-Wurttemberg, Germany). The hyperspectral camera was equipped with a DJI Ronin-MX three-axis gimbal stabilizer and installed on a DJI M600 PRO hexacopter

with global positioning system (GPS) and inertial navigation system modules (DJI, Shenzhen, China). The gimbal stabilizer ensured that the view angle of the camera was constant and acquired the nadir images. The hyperspectral camera captures 125 spectral bands in the range of 450-950 nm with a sampling interval of 4 nm. The light is split into two beams after passing through the camera lens. 80% of the entire light entering the hyperspectral camera creates a 50×50 pixels hyperspectral cube with a 12-bit dynamic range and the remaining 20% enters the panchromatic camera to create a panchromatic image with a resolution of 1000×1000 pixels (e.g., Aasen et al., 2015; Lu et al., 2020). After pan-sharpening the hyperspectral cube to the resolution of panchromatic image by the Cube-Pilot software (Cubert GmbH, Ulm, Baden-Wurttemberg, Germany), hyperspectral images with a size of 1000×1000 pixels can be generated.

The flight campaigns were performed between 10 a.m. and 2 p.m. in consistent weather conditions (cloudless or heavy cloud) to minimize changes in illumination. The hyperspectral camera was calibrated by a white and black board before flying. The flight height was 60 m, resulting in a spatial resolution of ca. 2 cm, and the flying speed was fixed at 6 m s^{-1}. The hyperspectral images were created automatically at a sampling time interval of 1 ms and the forward and side overlaps were set to 80% and 60%, respectively, under the control of a connected microcomputer. The hyperspectral images were orthographically stitched by the Agisoft PhotoScan software (Agisoft LLC, St. Petersburg, Russia) based on GPS coordinates or image textures. Finally, the region of interest was drawn from the sampling area on the obtained hyperspectral ortho-images. The mean spectrum of the destructive sampling area was used as the corresponding reflectance of each sample. The bands beyond 902 nm and below 470 nm were dropped in the later data analysis, due to the low spectral quality (Lu et al., 2020).

2.3 Features collections for leaf traits prediction

2.3.1 Canopy spectral features and vegetation indices

The raw bands from hyperspectral images were used as canopy spectral features. Additionally, a set of VIs was selected for predicting leaf traits. In our study, 37 narrowband hyperspectral VIs were collected, in which 6 were directly related to N, 16 were related to chlorophyll, and 15 were related to canopy traits like biomass, coverage or LAI (Table S2). One more red-edge position was added in the list of VIs (Table S2), which was regressed by the inverted Gaussian method (Miller et al., 1990). The wavelengths with the sampling interval of 4 nm in our study were linearly interpolated to 1 nm to match the needs of calculation of hyperspectral VIs.

2.3.2 Canopy texture information extraction

Texture information from each hyperspectral band was extracted by the commonly used grey level co-occurrence matrix algorithm (GLCM) (Haralick et al., 1973). Eight GLCM-based texture features, including mean, variance, homogeneity, contrast, dissimilarity, entropy, second moment and correlation, were computed using the ENVI 5.2 software (Exelis Visual Information Solutions, Boulder, Colorado, USA). To avoid complexity of computation, only four bands, 470, 550, 638, and 850 nm (for blue, green, red, and NIR bands, respectively), were selected here for canopy texture information extraction.

2.3.3 Crop development stage

As leaf traits were measured at various dates during crop growth and these traits varied in time, we considered to include crop development stage as a co-predictor in nonparametric regression algorithms. Development stage was simulated by the crop growth simulation model GECROS (Yin and Struik, 2017), in which the development stage at seedling emergence, flowering and maturity were denoted as dimensionless values 0.0, 1.0 and 2.0, respectively, and the effect of temperature fluctuations on rate of crop development was taken into account.

2.4 Nonparametric regression algorithms

Commonly used linear nonparametric regression algorithms like Partial Least Squares Regression (PLSR), two machine learning algorithms including Support Vector Regression (SVR) and Random Forest Regression

(RFR), and two DL-based algorithms DNN and CNN were implemented in the canopy leaf traits predictions (Fig. 2). The prepared feature information, including canopy reflectance (Ref), hyperspectral VIs, texture information (Tex), and development stage (DS), was selectively assembled and then compressed into a one-dimensional vector as the feature set (Table 3). Random assignment of instances was used for splitting the training and testing data for each model, in which 75% data at each growing stage was randomly selected and pooled in the training dataset and the remaining 25% was used for independent testing. Thus, the full-growth-stage models were built on the training set and validated on the testing set. All data analysis and model training were conducted in the Python environment. Regression models were implemented relying on the package of scikit-learn (0.24.1) (Pedregosa et al., 2011) and TensorFlow (2.5) (Abadi et al., 2015) in Python. Table S3 gives the specific properties and numerical settings of the hyperparameters for each regression algorithms. k -fold cross validated *RMSE* was minimized to tune the pivotal hyperparameters in machine learning models.

2.4.1 Partial Least Squares Regression (PLSR)

PLSR is characterized by the ability to perform regression modeling even when the independent variables have severe multiple correlations. PLSR also allows regression modeling even when there are fewer sample points than given variables, thereby allowing all original independent variables being included in the final model (Geladi and Kowalski, 1986). The only hyperparameter in PLSR optimized in this study was the number of potential components ("n_components", Table S3).

2.4.2 Support Vector Regression (SVR)

SVR has unique advantages in the case of small samples as well as nonlinear and high-dimensional inputs (Drucker et al., 1997). It improves the predictability by mapping low-dimensional samples into high-dimensional space and thus the non-linear inputs can be linearly separated by using a kernel function. SVR is efficient in finding sample information to achieve the best compromise between model complexity and learning ability.

2.4.3 Random Forest Regression (RFR)

RFR is a robust ensemble learning technique able to handle large numbers of input variables. RFR combines a large set of decision trees (Breiman, 2001). Together with the number of trees, tree traits and the number of input features can be optimized to get the best model (Table S3).

2.4.4 Artificial Neural Networks (ANNs)

Normally, an ANN is composed of an input layer, several hidden layers and an output layer and each layer contains a number of neurons. In this study, the fully connected feedforward DNN is based on simply increasing the depth (number of layers) of ANNs (Längkvist et al., 2014) (Fig. S1a). Fully connected 1-D CNN with several layers of convolution and pooling was designed as well (Fig. S1b). The stacking multiple layers are able to extract higher-order feature information (Längkvist et al., 2014). The optimum composition of hidden layers was determined by the minimum value of *RMSE* in validation dataset, while the number of neurons in each layer was asserted beforehand. Herein, the selected activation function for hidden layers was the Rectified Linear Unit with the form of f(z) = max(0, z) (LeCun et al., 2015). The weights of model neurons were initialized by the initialization method of He et al. (2015) and then updated by applying the gradient descent algorithm of the Adam optimizer. A reduced learning rate on plateau and early stopping were implemented as well to prevent overfitting.

2.5 Model performance evaluation

The performances of all models were evaluated by the results in the testing sets (unless specified), with the coefficient of determination (R^2) and the root mean square error (*RMSE*) with the following equation:

$$R^2 = 1 - \frac{\sum_{i=1}^{n} (y_i - \hat{y}_i)^2}{\sum_{i=1}^{n} (y_i - y)^2}$$

$$RMSE = \sqrt{\frac{1}{n}\sum_{i=1}^{n}(y_i - \hat{y}_i)^2}$$

where $\hat{y}_i$ is a predicted value, y_i is a measured value, y is the average value of measured values across the whole growing season, and n is the number of measurements.

Additionally, the normalized *RMSE* (*NRMSE*) was applied here as the metric of model performance evaluation in the needs of the comparison among crop species or among leaf traits, calculated by:

$$NRMSE = \frac{\text{RMSE}}{y}$$

3. Results

3.1 Canopy spectral reflectance and canopy and leaf N traits

Differences in canopy reflectance were observed across growth stages in the three crop species and the change tended to be similar in rice and wheat (Fig. 3a-c). Values of SLN in rice and wheat became lower with the progress of the growth stage, but SLN in maize even increased at maturity (Fig. 3d), which might be caused by the rapid decline in LAI associated with senescence of the upper leaves while the cob leaves remained green (Fig. S2). Values of LNC decreased from the tillering stage of rice and wheat or the early stem-elongating stage of maize onwards (Fig. 3e). Measured N_{canopy} in both rice and wheat reached the peak at the stem-elongating stage and then decreased until maturity, while the highest values of N_{canopy} in maize occurred at flowering (Fig. 3f). Unlike in rice and wheat, there was no significant difference in measured SLN, LNC and N_{canopy} between treatments in maize (results not shown), presumably because the residual N supply from soil was very high.

3.2 Correlograms of collected features with respect to leaf and canopy N traits

Among the three crops, the correlation coefficients (r) of N_{canopy} with canopy reflectance changed in a similar trend and slightly decreased when wavelength was between 680 nm and 710 nm, which belongs to the red-edge region (Fig. S3). SLN and LNC in rice showed weaker correlations than N_{canopy} with canopy reflectance in the NIR region and the r ranged from 0.15 to 0.27 and -0.06 to 0.11, respectively (Fig. S3a). Within the collected VIs, the highest values of r for SLN, LNC and N_{canopy}, with VIs were up to 0.77, 0.86 and 0.82 in rice, and 0.72, 0.93 and 0.95 in wheat (Fig. S4a-f). In maize, LNC displayed a weak correlation with collected VIs and the r ranged from -0.37 to 0.40 (Fig. S4g-i).

Regarding correlations with the texture information, leaf N traits were more correlated with the features extracted from blue, green and red bands than those from NIR in rice (Fig. S5a-d), while the higher correlations tended to be achieved from the bands of red and NIR in wheat and maize (Fig. S5e-l). The LNC in maize was highly correlated with the texture information from the NIR band and the highest value of r was up to 0.81 (Fig. S5l).

3.3 Performance of nonparametric regression algorithms

For SLN and LNC, PLSR and SVR models tended to improve their performance in rice and wheat when incorporating more features and the predicted LNC agreed with its measurements better than the predicted SLN among three crop species (Figs 4a-f, S7). For SLN in rice and wheat from PLSR and SVR, *NRMSE* decreased after incorporating VIs and Tex into the feature set of Ref, whereas *NRMSE* in maize tended to increase (Fig. 4a-c). For LNC, the performance of PLSR and SVR hardly changed in wheat while incorporating different feature types, but improved slightly in maize (Fig. 4e-f). For the predicted SLN and LNC, RFR tended to perform better than DNN among three crop species, albeit worse than PLSR and SVR (Fig. 4a-f). Although there was a chance that CNN performed better than other regression algorithms (Fig. 4a),

its performance lacked the consistency and tended to become worse when incorporating more feature types into the model (Fig. 4b-f).

For the predictions of N_{canopy}, PLSR and SVR always performed better than others and their performance tended to be consistently improved in the testing dataset when incorporating different types of features among three crop species (Fig. 4g-i). In detail, *NRMSE* of predicted N_{canopy} in rice from PLSR decreased from 0.352 to 0.303 after incorporating VIs into the feature set of Ref and hardly changed thereafter, while that of SVR further decreased to 0.291 after incorporating the feature of Tex (Fig. 4g). Also in wheat and maize, no increment of model performance was obtained while further incorporating the DS (Fig. 4h-i). Due to the increased complexity of their algorithms, RFR, DNN and CNN models were more likely to be overfitted in the training set (Fig. S6g-i) and their performance for N_{canopy} of the testing set in different crops tended to be highly variable while incorporating different types of features (Fig. 4g-i). For instance, after incorporating VIs into the feature set of Ref, *NRMSE* of predictedN_{canopy} in rice from DNN decreased from 0.345 to 0.305 and then increased to 0.388 after further incorporating the DS (Fig. 4g).

3.4 Performance in modelling canopy and leaf N by direct and indirect predictions

The best performing regression algorithm for predicting SLW and SLA changed among crop species, and in general, the predicted SLA agreed with its measurements better than SLW (Fig. 5, S8). The incorporation of feature sets also improved the predictions of SLW and SLA by PLSR and SVR in three crops (Fig. 5). Among different regression algorithms, PLSR and SVR performed better than others in rice (Fig. 5a, d), while DNN and CNN performed better in wheat (Fig. 5b, e). In maize, the predictions of SLW from RFR agreed with the measurements better, while PLSR and SVR performed better in the predictions of SLA (Fig. 5c, f).

As SLA was better predicted than SLW, the indirect predictions of SLN from SLA, SLN_{sla}, are only presented here (Table 4). Compared with the directly predicted SLN (SLN_{dir}), SLN_{sla} tended to agree better with the measurements, in which *NRMSE* decreased from 0.241, 0.254, and 0.189 to 0.240, 0.244 and 0.183, while R^2 increased from 0.699, 0.557 and 0.540 to 0.725, 0.583 and 0.611, for rice, wheat and maize, respectively. Both direct and indirect predictions from PLSR were better than those from SVR. Regarding the utilized feature sets, in rice and wheat, both predicted SLN agreed better with measurements while using the feature set of RefVIsTex. However, in maize, better performance was achieved when using the feature set of Ref only.

To upscale the predicted SLN to N_{canopy}, LAI was predicted well using the feature set of Ref or RefVIsTex while applying the regression algorithms of PLSR and SVR (Figs S9-S10). The indirect predictions of $N_{canopy,SLNdir}$ and$N_{canopy,SLNsla}$ were estimated from SLN_{dir} and SLN_{sla}, respectively. Using more features from Ref to RefVIsTex universally improved directly or indirectly predicted N_{canopy}, except for the slight decrease in the indirect predictions from SVR in wheat and maize (Fig. 6). Therefore, for further analysis, we only show the predictions from applying the feature set of RefVIsTex. Within the comparison between direct and indirect predictions,$N_{canopy,dir}$ in wheat agreed with the measurements better than others, while in rice and maizeN_{canopy} tended to be better predicted via the indirect method ($N_{canopy,SLNdir}$). For instance, compared with $N_{canopy,dir}$ from PLSR, *NRMSE*of $N_{canopy,SLNdir}$ in rice decreased from 0.307 to 0.286 (Fig. 6a). Between the two indirect predictions, the predicted$N_{canopy,SLNdir}$ generally had a lower NRMSE in the three crop species than the predicted$N_{canopy,SLNsla}$ (Fig. 6).

3.5 Predicted N_{canopy} along stages of the whole season

The predicted N_{canopy} values in rice, wheat and maize were mapped in the whole experimental area and illustrated for different growing stages (Figs 7, S11-S12). Taking rice as an example, in line with the field measurements (Fig. 3f), the highestN_{canopy} occurred at stem elongation and remarkable differences were shown between experimental plots (Fig. 7b). Such differences among treatments gradually narrowed after stem elongation (Fig. 7b-f). A similar trend was observed in mappedN_{canopy} of wheat (Fig. S11), in agreement with its field measurements (Fig. 3f). In maize, the differences inN_{canopy} among growing stages were predicted well (Fig. S12). The hardly observed differences of predictedN_{canopy} between experimental plots also agreed with the fact that there was no significant difference in measuredN_{canopy} between treatments

(Figs 3f, S12). Moreover, the differences in crop growth status within an experimental plot was also noticeable (Figs 7, S11-S12).

4. Discussion

Leaf and canopy N contents across growing stages for three major field crops were predicted from UAV based hyperspectral image features, by adopting different nonparametric regression algorithms and predicting pathways (direct vs. indirect). The mapped N_{canopy} across successive growth stages demonstrates the potential utilization of the prediction models.

4.1 Comparison of direct and indirect predictions

As SLA and SLW are reciprocals of each other, the difference between them has been hardly noticed. But there are still some debates about predicting them from remote sensing images. For instance, SLW could be predicted well and the reported R^2 values were ca. 0.90 (Ecarnot et al., 2013; Silva-Perez et al., 2018). However, Ali et al. (2017) indicated that SLA tended to be more correlated with leaf reflectance than SLW, whereas Hussain et al. (2020) showed that the predictions of SLW matched its measurements better than the predictions of SLA did. With crop growth, our data range of SLW tended to become wider than that of SLA in three crop species (results not shown) whereas the differences of canopy reflectance between treatments tended to be diminished (Fig. 3a-c), which might contribute to the better predicted SLA than that of SLW (Figs 5, S8).

Both SLN and LNC are common leaf level indicators to monitor leaf N. As the components in whole leaf thickness accounts for the light reflection or absorption, SLN is supposed to be better predicted than LNC (Baret and Fourty, 1997). However, our results showed that the predicted LNC agreed with its measurements better than the predicted SLN did (Figs 4a-f, S7), in line with the previous results of Ecarnot et al. (2013) and Li et al. (2018) using measured raw reflectance spectra. Under N shortage, leaf weight increases because of accumulation of starch and cell wall material (McDonald et al., 1986; Terry et al., 1983) and thus SLA or SLW varies significantly (Jones and Hesketh, 1980). As leaf expansion is limited, the change of leaf N status is reflected less in SLN than in LNC. Moreover, as SLN is normally determined from LNC and SLA, meaning that it requires more measurement steps to determine SLN than to determine LNC, data for SLN must contain more measurement noise than for LNC. Due to the better predicted LNC and SLA, the indirectly predicted SLN_{sla} tended to match measurements than directly predicted SLN_{dir} (Table 4). However, when upscaling to canopy level, the indirectly predicted N_{canopy} from SLN_{sla} became worse than that from SLN_{dir} (Fig. 6). As SLN_{sla} was estimated from predicted LNC and SLA, this result supported the assertion by Kattenborn et al. (2019) that area-based leaf traits, like SLN, are more suitable for upscaling from leaf to canopy level than mass-based leaf traits, like LNC, as less regression error was introduced. The indirect predictions of $N_{\text{canopy,SLN}}$ in rice and maize tended to agree with measurements than the directly predicted $N_{\text{canopy,dir}}$ (Fig. 6). Even though the indirect methods achieved better prediction in our results (Table 4, Fig. 6), as more regression processes were introduced, the results might be more uncertain (Malenovský et al., 2019). Thus, the uncertainty of the regression processes should be further investigated.

4.2 Contribution of feature types in canopy and leaf nitrogen prediction

Fusing different types of features contributes to plant N traits prediction. Besides the raw bands, VIs have also been considered as supplementary information serving as canopy spectral features (Maimaitijiang et al., 2020). There were tight correlations between VIs and leaf N traits (Fig. S4). However, with Ref features used as the baseline, adding VIs to the model did not always yield better prediction (Fig. 4), which might be caused by the introduced noisy information from VIs and/or the correlations between Ref and VIs features. Due to the different changing rate in crop biomass accumulation or N uptake between before and after heading, the predictability using hyperspectral VIs could be significantly influenced (Li et al., 2010; Yu et al., 2013). On the other hand, as VIs are normally derived from several bands (Table S2), the information provided from VIs might be limited compared with that from Ref in the full spectrum (Wang et al., 2021). From the extracted canopy texture features, the additional information associated with spatial canopy architecture and structure characteristics is potentially provided (Colombo, 2003). The fusion of canopy texture information

benefits the predictions not only of the canopy traits like LAI and biomass (Liu et al., 2021; Zheng et al., 2018b), but also of crop N status like leaf chlorophyll and plant aboveground N content (Qiao et al., 2020; Zheng et al., 2018a). Similar to these previous studies, our results also showed that fusing canopy texture information contributed to the prediction of leaf N traits, especially for the regression models based on PLSR and SVR (Table 4, Figs 4, 6).

Although both measured canopy reflectance and leaf N traits changed across growth stages (Fig. 3), the performance of the regressing models in predicting leaf N traits hardly improved after directly incorporating DS into the models (Fig. 4). The feature of DS might be utilized in a more proper way. For instance, Li et al. (2022) found that the coefficient values (slope and intercept) of ordinary least squares regression of aboveground biomass in wheat with VIs had a strong relationship with phenological stages. With the calibrated slopes and intercepts at different stages, aboveground biomass can be well estimated over the entire growing season (Li et al., 2022). Moreover, the appropriate digital indicator of crop growth stages is of importance as well. The simulated DS in this study is only one way of quantifying development stages, which is calculated from hourly temperatures, using a bell-shaped temperature response function capturing base, optimum and ceiling temperatures (Yin and van Laar, 2005). It is similar to growth stages with the Zadoks scale, using a numeric system between 0 and 100 representing stages from sowing to harvest (Zadoks et al., 1974). Li et al. (2022) showed that compared with the thermal-based digital indicator of growth stages, growth stages with the Zadoks scale performed better in the prediction of aboveground biomass of wheat.

4.3 Characteristics of regression algorithms in canopy and leaf nitrogen prediction

The performance of five popular nonparametric regression algorithms were evaluated for N traits in three major field crops in this study. Among these methods, PLSR used the least number of hyperparameters and SVR next to it, compared with RFR, DNN and CNN that have many hyperparameters (Table S3) and thus, in principle, should have the more flexibility in the prediction of leaf N traits. However, our results showed that PLSR and SVR tended to be more stable and PLSR was likely to achieve the best model performance in the prediction ofN_{canopy}, as well as SLN and LNC (Figs 4, S7), in line with the results in the prediction of LNC in wheat (Yao et al., 2015). This might be caused by the limited size of our dataset, as PLSR is known to be more effective than others, when the number of samples is smaller than the number of variables (Geladi and Kowalski, 1986). With nearly 1000 samples, DNN based yield prediction models systematically performed better than PLSR and SVR based models while increasing feature types (Maimaitijiang et al., 2020). Moreover, with more than 7000 samples from different years and locations, CNN provided higher accuracy in LNC prediction in grass (Pullanagari et al., 2021). Thus, as the numerous combinations of hyperparameters in RFR and of hidden layers and neuro numbers in DNN and CNN have already been trialed in this study (Table S3, Fig. S1), increasing the number of samples might be the essential for improving the predictability of DNN and CNN.

5. **Conclusions**

We evaluated the prediction of area- and mass-based leaf N traits using different regression algorithms and feature sets extracted from hyperspectral images for three major crops, rice, wheat and maize. Our results showed that for the prediction of N traits at leaf level, SLN and LNC, and at canopy level N_{canopy} using the limited size of the dataset, regression algorithms of PLSR and SVR tended to perform better than others, and the incorporation of different types of features, like canopy spectral, VIs and texture information, helped improve model performance. The regression algorithm of PLSR performed slightly better than SVR in the prediction ofN_{canopy}. PredictingN_{canopy} in an indirect way by upscaling SLN contributed to the further improvement of prediction ofN_{canopy}, compared with the directly predictedN_{canopy}, although the regression process might be more uncertain. These results provide useful information for the next-step work that will couple the real-time accurately retrieved leaf N traits into dynamic crop models so as to predict the real-time growth status more accurately, given that canopy photosynthesis is directly linked with crop N status and primarily determines crop growth rates. This would better enable crop models as a decision-making tool to guide farmers for in situ field N management targeting the maximal yield or resource use efficiency.

Appendix A. Supplementary data

Supplementary tables and figures related to this article can be found in the supplementary material.

References

Abadi, M., Agarwal, A., Barham, P., Brevdo, E., Chen, Z., Citro. Craig, Corrado, G. S., Davis, A., Dean, J., Devin, M., Ghemawat, S., Goodfellow, I., Harp, A., Irving, G., Isard, M., Jozefowicz, R., Jia, Y., Kaiser, L., Kudlur, M., Levenberg, J., Mané, D., Schuster, M., Monga, R., Moore, S., Murray, D., Olah, C., Shlens, J., Steiner, B., Sutskever, I., Talwar, K., Tucker, P., Vanhoucke, V., Vasudevan, V., Viégas, F., Vinyals, O., Warden, P., Wattenberg, M., Wicke, M., Yu, Y., & Zheng, X. (2015). TensorFlow: A System for Large-Scale Machine Learning. Software available from tensflow.org.

Ali, A. M., Darvishzadeh, R., Skidmore, A. K., & van Duren, I. (2017). Specific leaf area estimation from leaf and canopy reflectance through optimization and validation of vegetation indices. *Agricultural and Forest Meteorology, 236* , 162-174. doi:10.1016/j.agrformet.2017.01.015

Aasen, H., Burkart, A., Bolten, A., & Bareth, G. (2015). Generating 3D hyperspectral information with lightweight UAV snapshot cameras for vegetation monitoring: From camera calibration to quality assurance.*ISPRS Journal of Photogrammetry and Remote Sensing, 108* , 245-259. doi:10.1016/j.isprsjprs.2015.08.002

Atzberger, C., Guérif, M., Baret, F., & Werner, W. (2010). Comparative analysis of three chemometric techniques for the spectroradiometric assessment of canopy chlorophyll content in winter wheat. *Computers and Electronics in Agriculture, 73* , 165-173. doi:10.1016/j.compag.2010.05.006

Baret, F., & Fourty, T. (1997). Radiometric estimates of nitrogen status of leaves and canopies *Diagnosis of nitrogen status in crops* (pp. 201-227): Springer.

Beeckman, F., Motte, H., & Beeckman, T. (2018). Nitrification in agricultural soils: impact, actors and mitigation. *Current Opinion in Biotechnology, 50* , 166-173.

Berger, K., Verrelst, J., Féret, J.-B., Wang, Z., Wocher, M., Strathmann, M., Danner, M., Mauser, W., & Hank, T. (2020). Crop nitrogen monitoring: Recent progress and principal developments in the context of imaging spectroscopy missions. *Remote Sensing of Environment, 242* , 111758. doi:10.1016/j.rse.2020.111758

Boote, K. J., Jones, J. W., Hoogenboom, G., & Pickering, N. B. (1998). The CROPGRO model for grain legumes *Understanding options for agricultural production* (pp. 99-128): Springer.

Breiman, L. (2001). Random forests. *Machine learning, 45* , 5-32.

Colombo, R. (2003). Retrieval of leaf area index in different vegetation types using high resolution satellite data. *Remote Sensing of Environment, 86* , 120-131. doi:10.1016/s0034-4257(03)00094-4

Davidson, E. A. (2009). The contribution of manure and fertilizer nitrogen to atmospheric nitrous oxide since 1860. *Nature Geoscience, 2* , 659-662.

Drucker, H., Burges, C. J., Kaufman, L., Smola, A., & Vapnik, V. (1997). Support vector regression machines. In M. Mozer, J. Jordan, & T. Petscbe (Eds.), *Neural information processing systems 9* (pp. 155-161). Cambridge, MA: MIT Press.

Ecarnot, M., Compan, F., & Roumet, P. (2013). Assessing leaf nitrogen content and leaf mass per unit area of wheat in the field throughout plant cycle with a portable spectrometer. *Field Crops Research, 140* , 44-50. doi:10.1016/j.fcr.2012.10.013

Evans, J. R. (1983). Nitrogen and photosynthesis in the flag leaf of wheat (Triticum aestivum L.). *Plant Physiology, 72* , 297-302.

FAO. (2020). *World Food and Agriculture - Statistical Yearbook 2020* . Rome.

Fu, Y., Yang, G., Li, Z., Li, H., Li, Z., Xu, X., Song, X., Zhang, Y., Duan, D., Zhao, C., & Chen, L. (2020). Progress of hyperspectral data processing and modelling for cereal crop nitrogen monitoring. *Computers and Electronics in Agriculture, 172* , 105321. doi:10.1016/j.compag.2020.105321

Geladi, P., & Kowalski, B. R. (1986). Partial least-squares regression: a tutorial. *Analytica Chimica Acta, 185* , 1-17.

Haralick, R. M., Shanmugam, K., & Dinstein, I. H. (1973). Textural features for image classification. *IEEE Transactions on systems, man, and cybernetics* , 610-621.

He, K., Zhang, X., Ren, S., & Sun, J. (2015). *Delving deep into rectifiers: Surpassing human-level performance on imagenet classification* .

Homolová, L., Malenovský, Z., Clevers, J. G. P. W., García-Santos, G., & Schaepman, M. E. (2013). Review of optical-based remote sensing for plant trait mapping. *Ecological Complexity, 15* , 1-16. doi:10.1016/j.ecocom.2013.06.003

Horler, D. N. H., Dockray, M., & Barber, J. (1983). The red edge of plant leaf reflectance. *International Journal of Remote Sensing, 4* , 273-288.

Hussain, S., Gao, K., Din, M., Gao, Y., Shi, Z., & Wang, S. (2020). Assessment of UAV-Onboard Multispectral Sensor for Non-Destructive Site-Specific Rapeseed Crop Phenotype Variable at Different Phenological Stages and Resolutions. *Remote Sensing, 12* (3). doi:10.3390/rs12030397

Jin, X., Kumar, L., Li, Z., Feng, H., Xu, X., Yang, G., & Wang, J. (2018). A review of data assimilation of remote sensing and crop models. *European Journal of Agronomy, 92* , 141-152. doi:10.1016/j.eja.2017.11.002

Jones, J. W., & Hesketh, J. D. (1980). Predicting leaf expansion. In J. D. Hesketh & J. W. Jones (Eds.), *Predicting Photosynthesis for Ecosystem Models. Volume II* (pp. 85-122). Boca Raton, FL: CRC Press.

Kattenborn, T., Schiefer, F., Zarco-Tejada, P., & Schmidtlein, S. (2019). Advantages of retrieving pigment content [µg/cm2] versus concentration [%] from canopy reflectance. *Remote Sensing of Environment, 230* . doi:10.1016/j.rse.2019.05.014

Khoury, C. K., Bjorkman, A. D., Dempewolf, H., Ramirez-Villegas, J., Guarino, L., Jarvis, A., Rieseberg, L. H., & Struik, P. C. (2014). Increasing homogeneity in global food supplies and the implications for food security. *Proc Natl Acad Sci U S A, 111* , 4001-4006. doi:10.1073/pnas.1313490111

Kropff, M. J., Van Laar, H. H., & Matthews, R. B. (1994). *ORYZA1: An ecophysiological model for irrigated rice production* . Wageningen: DLO-Research Institute for Agrobiology and Soil Fertility.

Längkvist, M., Karlsson, L., & Loutfi, A. (2014). A review of unsupervised feature learning and deep learning for time-series modeling. *Pattern Recognition Letters, 42* , 11-24. doi:10.1016/j.patrec.2014.01.008

LeCun, Y., Bengio, Y., & Hinton, G. (2015). Deep learning. *Nature, 521* , 436-444. doi:10.1038/nature14539

Lemaire, G., Jeuffroy, M.-H., & Gastal, F. (2008). Diagnosis tool for plant and crop N status in vegetative stage: Theory and practices for crop N management. *European Journal of Agronomy, 28* , 614-624. doi:10.1016/j.eja.2008.01.005

Li, D., Wang, X., Zheng, H., Zhou, K., Yao, X., Tian, Y., Zhu, Y., Cao, W., & Cheng, T. (2018). Estimation of area- and mass-based leaf nitrogen contents of wheat and rice crops from water-removed spectra using continuous wavelet analysis. *Plant Methods, 14* , 76. doi:10.1186/s13007-018-0344-1

Li, F., Miao, Y., Hennig, S. D., Gnyp, M. L., Chen, X., Jia, L., & Bareth, G. (2010). Evaluating hyperspectral vegetation indices for estimating nitrogen concentration of winter wheat at different growth stages. *Precision Agriculture, 11* , 335-357. doi:10.1007/s11119-010-9165-6

Li, Z., Zhao, Y., Taylor, J., Gaulton, R., Jin, X., Song, X., Li, Z., Meng, Y., Chen, P., Feng, H., Wang, C., Guo, W., Xu, X., Chen, L., & Yang, G. (2022). Comparison and transferability of thermal, temporal

and phenological-based in-season predictions of above-ground biomass in wheat crops from proximal crop reflectance data. *Remote Sensing of Environment, 273* , 112967. doi:10.1016/j.rse.2022.112967

Liu, H., Zhu, H., & Wang, P. (2016). Quantitative modelling for leaf nitrogen content of winter wheat using UAV-based hyperspectral data.*International Journal of Remote Sensing, 38* , 2117-2134. doi:10.1080/01431161.2016.1253899

Liu, S., Jin, X., Nie, C., Wang, S., Yu, X., Cheng, M., Shao, M., Wang, Z., Tuohuti, N., Bai, Y., & Liu, Y. (2021). Estimating leaf area index using unmanned aerial vehicle data: shallow vs. deep machine learning algorithms. *Plant Physiology, 187* , 1551-1576. doi:10.1093/plphys/kiab322

Lu, J., Li, W., Yu, M., Zhang, X., Ma, Y., Su, X., Yao, X., Cheng, T., Zhu, Y., Cao, W., & Tian, Y. (2020). Estimation of rice plant potassium accumulation based on non-negative matrix factorization using hyperspectral reflectance. *Precision Agriculture, 22* , 51-74. doi:10.1007/s11119-020-09729-z

Maimaitijiang, M., Sagan, V., Sidike, P., Hartling, S., Esposito, F., & Fritschi, F. B. (2020). Soybean yield prediction from UAV using multimodal data fusion and deep learning. *Remote Sensing of Environment, 237* , 111599. doi:10.1016/j.rse.2019.111599

Malenovský, Z., Homolová, L., Lukeš, P., Buddenbaum, H., Verrelst, J., Alonso, L., Schaepman, M. E., Lauret, N., & Gastellu-Etchegorry, J.-P. (2019). Variability and Uncertainty Challenges in Scaling Imaging Spectroscopy Retrievals and Validations from Leaves Up to Vegetation Canopies. *Surveys in Geophysics, 40* , 631-656. doi:10.1007/s10712-019-09534-y

Marshall, M., & Thenkabail, P. (2015). Advantage of hyperspectral EO-1 Hyperion over multispectral IKONOS, GeoEye-1, WorldView-2, Landsat ETM+, and MODIS vegetation indices in crop biomass estimation. *ISPRS Journal of Photogrammetry and Remote Sensing, 108* , 205-218. doi:10.1016/j.isprsjprs.2015.08.001

McDonald, A. J. S., Lohammar, T., & Ericsson, A. (1986). Growth response to step-decrease in nutrient availability in small birch (Betula pendula Roth). *Plant, Cell & Environment, 9* , 427-432.

Miller, J. R., Hare, E. W., & Wu, J. (1990). Quantitative characterization of the vegetation red edge reflectance 1. An inverted-Gaussian reflectance model. *International Journal of Remote Sensing, 11* , 1755-1773. doi:10.1080/01431169008955128

Moharana, S., & Dutta, S. (2016). Spatial variability of chlorophyll and nitrogen content of rice from hyperspectral imagery. *ISPRS Journal of Photogrammetry and Remote Sensing, 122* , 17-29. doi:10.1016/j.isprsjprs.2016.09.002

Mulla, D. J. (2013). Twenty five years of remote sensing in precision agriculture: Key advances and remaining knowledge gaps. *Biosystems Engineering, 114* , 358-371. doi:10.1016/j.biosystemseng.2012.08.009

Ohyama, T. (2010). Nitrogen as a major essential element of plants. In T. Ohyama & K. Sueyoshi (Eds.), *Nitrogen Assimilation in Plants*(pp. 1–18): Research Signpost.

Padilla, F. M., Gallardo, M., & Manzano-Agugliaro, F. (2018). Global trends in nitrate leaching research in the 1960–2017 period.*Science of the Total Environment, 643* , 400-413.

Pedregosa, F., Varoquaux, G., Gramfort, A., Michel, V., Thirion, B., Grisel, O., Blondel, M., Prettenhofer, P., Weiss, R., Dubourg, V., Vanderplas, J., Passos, A., Cournapeau, D., Brucher, M., Perrot, M., & Duchesnay, E. (2011). Scikit-learn: Machine learning in Python.*Journal of machine Learning research* , 2825-2830.

Peng, S., Cassman, K. G., & Kropff, M. J. (1995). Relationship between leaf photosynthesis and nitrogen content of field-grown rice in tropics.*Crop science, 35* , 1627-1630.

Poorter, H., & Evans, J. R. (1998). Photosynthetic nitrogen-use efficiency of species that differ inherently in specific leaf area.*Oecologia, 116* , 26-37.

Pullanagari, R. R., Dehghan-Shoar, M., Yule, I. J., & Bhatia, N. (2021). Field spectroscopy of canopy nitrogen concentration in temperate grasslands using a convolutional neural network. *Remote Sensing of Environment, 257* , 112353. doi:10.1016/j.rse.2021.112353

Qiao, L., Gao, D., Zhang, J., Li, M., Sun, H., & Ma, J. (2020). Dynamic Influence Elimination and Chlorophyll Content Diagnosis of Maize Using UAV Spectral Imagery. *Remote Sensing, 12* (16). doi:10.3390/rs12162650

Raj, R., Walker, J. P., Pingale, R., Banoth, B. N., & Jagarlapudi, A. (2021). Leaf nitrogen content estimation using top-of-canopy airborne hyperspectral data. *International Journal of Applied Earth Observation and Geoinformation, 104* , 102584. doi:10.1016/j.jag.2021.102584

Schröder, J. J., Neeteson, J. J., Oenema, O., & Struik, P. C. (2000). Does the crop or the soil indicate how to save nitrogen in maize production?: Reviewing the state of the art. *Field Crops Research, 66* , 151-164.

Serbin, S. P., Dillaway, D. N., Kruger, E. L., & Townsend, P. A. (2012). Leaf optical properties reflect variation in photosynthetic metabolism and its sensitivity to temperature. *Journal of Experimental Botany, 63* , 489-502. doi:10.1093/jxb/err294

Silva-Perez, V., Molero, G., Serbin, S. P., Condon, A. G., Reynolds, M. P., Furbank, R. T., & Evans, J. R. (2018). Hyperspectral reflectance as a tool to measure biochemical and physiological traits in wheat. *J Exp Bot, 69* (3), 483-496. doi:10.1093/jxb/erx421

Skiba, U. M. (2014). Nitrous oxide, climate change and agriculture. *CAB Reviews: Perspectives in Agriculture, Veterinary Science, Nutrition and Natural Resources, 9* . doi:10.1079/pavsnnr20149010

Terry, N., Waldron, L. J., & Taylor, S. E. (1983). Environmental influences on leaf expansion. In J. E. Dale & F. L. Milthorpe (Eds.), *The growth and functioning of leaves* (pp. 179-205). Cambridge: Cambridge University Press.

Thomas, J. R., & Oerther, G. F. (1972). Estimating nitrogen content of sweet pepper leaves by reflectance measurements. *Agronomy Journal, 64* , 11-13.

Verrelst, J., Malenovský, Z., Van der Tol, C., Camps-Valls, G., Gastellu-Etchegorry, J.-P., Lewis, P., North, P., & Moreno, J. (2019). Quantifying Vegetation Biophysical Variables from Imaging Spectroscopy Data: A Review on Retrieval Methods. *Surveys in Geophysics, 40* , 589-629. doi:10.1007/s10712-018-9478-y

Wang, D., Rianti, W., Gálvez, F., van der Putten, P. E. L., Struik, P. C., & Yin, X. (2022). Estimating photosynthetic parameter values of rice, wheat, maize and sorghum to enable smart crop cultivation. *Crop and Environment, 1* (2), 119-132. doi:10.1016/j.crope.2022.05.004

Wang, L., Chen, S., Li, D., Wang, C., Jiang, H., Zheng, Q., & Peng, Z. (2021). Estimation of Paddy Rice Nitrogen Content and Accumulation Both at Leaf and Plant Levels from UAV Hyperspectral Imagery. *Remote Sensing, 13* , 2956. doi:10.3390/rs13152956

Weiss, M., Jacob, F., & Duveiller, G. (2020). Remote sensing for agricultural applications: A meta-review. *Remote Sensing of Environment, 236* , 111402.

Yao, X., Huang, Y., Shang, G., Zhou, C., Cheng, T., Tian, Y., Cao, W., & Zhu, Y. (2015). Evaluation of Six Algorithms to Monitor Wheat Leaf Nitrogen Concentration. *Remote Sensing, 7* , 14939-14966. doi:10.3390/rs71114939

Yin, X., & Struik, P. C. (2017). Can increased leaf photosynthesis be converted into higher crop mass production? A simulation study for rice using the crop model GECROS. *Journal of Experimental Botany, 68* , 2345-2360. doi:10.1093/jxb/erx085

Yin, X., Struik, P. C., Romero, P., Harbinson, J., Evers, J. B., PE, V. D. P., & Vos, J. (2009). Using combined measurements of gas exchange and chlorophyll fluorescence to estimate parameters of a biochemical C3 pho-

tosynthesis model: a critical appraisal and a new integrated approach applied to leaves in a wheat (Triticum aestivum) canopy. *Plant, Cell and Environment, 32* , 448-464. doi:10.1111/j.1365-3040.2009.01934.x

Yin, X., & van Laar, H. H. (2005). *Crop systems dynamics: an ecophysiological simulation model for genotype-by-environment interactions* . Wageningen, the Netherlands: Wageningen Academic Publishers.

Yu, K., Li, F., Gnyp, M. L., Miao, Y., Bareth, G., & Chen, X. (2013). Remotely detecting canopy nitrogen concentration and uptake of paddy rice in the Northeast China Plain. *ISPRS Journal of Photogrammetry and Remote Sensing, 78* , 102-115. doi:10.1016/j.isprsjprs.2013.01.008

Zadoks, J. C., Chang, T. T., & Konzak, C. F. (1974). A decimal code for the growth stages of cereals. *Weed research, 14* , 415-421.

Zeng, F., Zuo, Z., Mo, J., Chen, C., Yang, X., Wang, J., Wang, Y., Zhao, Z., Chen, T., Li, Y., Zhang, Z., Hu, Z., & Xu, H. (2021). Runoff Losses in Nitrogen and Phosphorus From Paddy and Maize Cropping Systems: A Field Study in Dongjiang Basin, South China. *Frontiers in Plant Science, 12* , 675121. doi:10.3389/fpls.2021.675121

Zheng, H., Cheng, T., Li, D., Yao, X., Tian, Y., Cao, W., & Zhu, Y. (2018a). Combining Unmanned Aerial Vehicle (UAV)-Based Multispectral Imagery and Ground-Based Hyperspectral Data for Plant Nitrogen Concentration Estimation in Rice. *Frontiers in Plant Science, 9* , 936. doi:10.3389/fpls.2018.00936

Zheng, H., Cheng, T., Zhou, M., Li, D., Yao, X., Tian, Y., Cao, W., & Zhu, Y. (2018b). Improved estimation of rice aboveground biomass combining textural and spectral analysis of UAV imagery. *Precision Agriculture, 20* , 611-629. doi:10.1007/s11119-018-9600-7

Table 1. List of acronyms of leaf traits at the leaf and canopy level with their definitions or calculations, and units.

Acronym	Definition or calculation	Unit
LAI	Leaf area index	m^2 leaf (m^2 ground)$^{-1}$
LNC	Leaf nitrogen concentration	g N (g dry matter)$^{-1}$
SLA	Specific leaf area	m^2 leaf (g dry matter)$^{-1}$
SLN	Specific leaf nitrogen content	g N (m^2 leaf)$^{-1}$
SLN_{dir}	SLN directly predicted from hyperspectral images	g N (m^2 leaf)$^{-1}$
SLN_{sla}	SLN indirectly predicted as the predicted LNC divided by the predicted SLA	g N (m^2 leaf)$^{-1}$
SLW	Specific leaf weight (= 1/SLA)	g dry matter (m^2 leaf)$^{-1}$
N_{canopy}	Leaf nitrogen content at the canopy level	g N (m^2 ground)$^{-1}$
$N_{canopy,dir}$	N_{canopy} directly predicted from hyperspectral images	g N (m^2 ground)$^{-1}$
$N_{canopy,SLNdir}$	N_{canopy} indirectly predicted as the SLN_{dir} divided by the predicted LAI	g N (m^2 ground)$^{-1}$
$N_{canopy,SLNsla}$	N_{canopy} indirectly predicted as the SLN_{sla} divided by the predicted LAI	g N (m^2 ground)$^{-1}$

Table 2. Sampling dates and the number of destructive field samples at corresponding growth stages of rice, maize and wheat.

Growth stage	Rice	No. of samples	Maize	No. of samples	Winter w
Tillering stage/ Early stem-elongating stage	22 July	24	7 July	19	22 March
Stem-elongating stage	15 August	24	20 July	19	8 April
Flowering stage	8 September	24	4 August	19	27 April
Grain-filling stage	21 September	24	25 August	19	10 May
Grain-filling stage	10 October	24	7 September	19	25 May
Maturity	30 October	24	23 September	18	4 June
Total no. of samples		144		113	

Table 3. Description of the combinations of feature sets from hyperspectral images and crop model simulations.

Acronym	Feature type	Feature number
Ref	Canopy reflectance	109
RefVIs	Canopy reflectance + Vegetation indices	146
RefVIsTex	Canopy reflectance + Vegetation indices + Texture information	178
All	Canopy reflectance + Vegetation indices + Texture information + Development stage	179

Table 4: The prediction performance in the testing dataset of directly and indirectly predicted specific leaf nitrogen (SLN) in rice, wheat and maize using feature sets of Ref and RefVIsTex (see Table 3 for their definition) and applying the regression algorithms of Partial Least Squares Regression (PLSR) and Support Vector Regression (SVR)[a].

Method	Feature set		Rice		Wheat		Maize	
			SLN_{dir}	SLN_{sla}	SLN_{dir}	SLN_{sla}	SLN_{dir}	SLN_{sla}
PLSR	Ref	R^2	**0.666**	0.659	0.462	**0.564**	0.540	**0.611**
		NRMSE	**0.254**	0.266	0.281	**0.251**	0.189	**0.183**
	RefVIsTex	R^2	0.699	**0.725**	0.557	**0.583**	**0.471**	0.440
		NRMSE	0.241	**0.240**	0.254	**0.244**	**0.200**	0.207
SVR	Ref	R^2	0.546	**0.626**	0.522	**0.533**	0.432	**0.582**
		NRMSE	0.301	**0.276**	0.258	**0.256**	0.215	**0.183**
	RefVIsTex	R^2	**0.677**	0.661	**0.582**	0.563	0.369	**0.481**
		NRMSE	**0.250**	0.262	**0.243**	0.246	0.224	**0.197**

[a] For each set of analysis, there is a directly predicted SLN (SLN_{dir}) and an indirectly predicted SLN (SLN_{sla}), the SLN calculated as the predicted leaf nitrogen concentration divided by the predicted specific leaf area (see also Table 1). The regression algorithms for the prediction of SLA were specified as SVR, Convolution Neural Network, and PLSR for rice, wheat and maize, respectively, as these algorithms yielded the best performance for the three crops. For the better predicted SLN in the direct vs indirect predictions' comparison, its correspondingR^2 and NRMSE values are given in bold.

Hosted file

`image1.emf` available at https://authorea.com/users/701034/articles/689314-estimating-leaf-and-canopy-nitrogen-contents-in-major-field-crops-across-the-growing-season-from-hyperspectral-images-using-nonparametric-regression

Fig. 1. Study sites of the field experiments of maize (a), wheat (b) and rice (c). The true color images (Red: 638 nm, Green: 550 nm, Blue: 470 nm) at the stem-elongating stage are illustrated here. N0, N40, N80, N160, N240, N320 and N400 denote different nitrogen (N) application rates (see Table S1 for details).

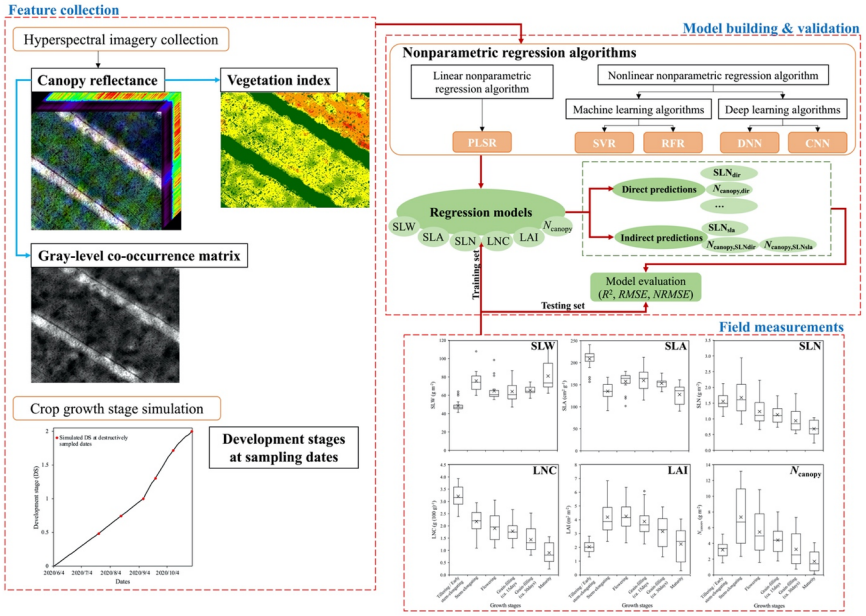

Fig. 2. The workflow diagram of data acquisition, feature collection, and data analysis in this study. Nonparametric regression algorithms are: PLSR = Partial Least Squares Regression, SVR = Support Vector Regression, RFR = Random Forest Regression, DNN = Deep Neural Network, CNN = Convolution Neural Network. Crop traits are: SLW = specific leaf weight, SLA = specific leaf area, SLN = specific leaf nitrogen, LNC = leaf nitrogen concentration, LAI = leaf area index, N_{canopy} = canopy nitrogen content. $N_{\text{canopy,dir}}$ and SLN_{dir} represent the direct predictions of N_{canopy} and SLN, respectively. Within the indirect predictions, SLN_{sla} was calculated as the predicted LNC divided by the predicted SLA, $N_{\text{canopy,SLNdir}}$ was derived from predicted LAI and SLN_{dir}, and $N_{\text{canopy,SLNsla}}$ was derived from predicted LAI and SLN_{sla} (indirectly predicted SLN via SLA).

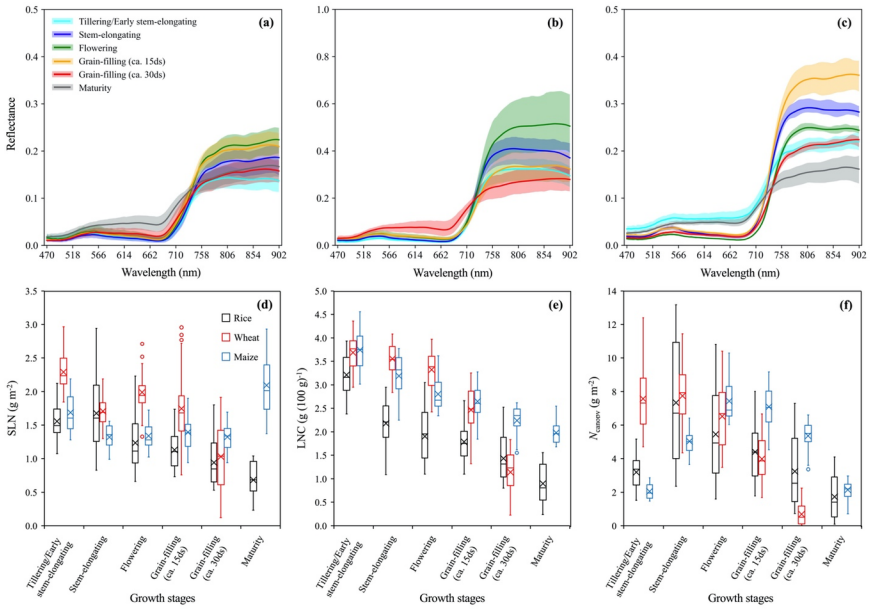

Fig. 3. Range of the collected canopy reflectance of rice (a), wheat (b) and maize (c), and the data distribution of destructively sampled specific leaf nitrogen (SLN) (d), leaf nitrogen concentration (LNC) (e), and canopy nitrogen content (N_{canopy}) (f) at different stages during the whole growing season.

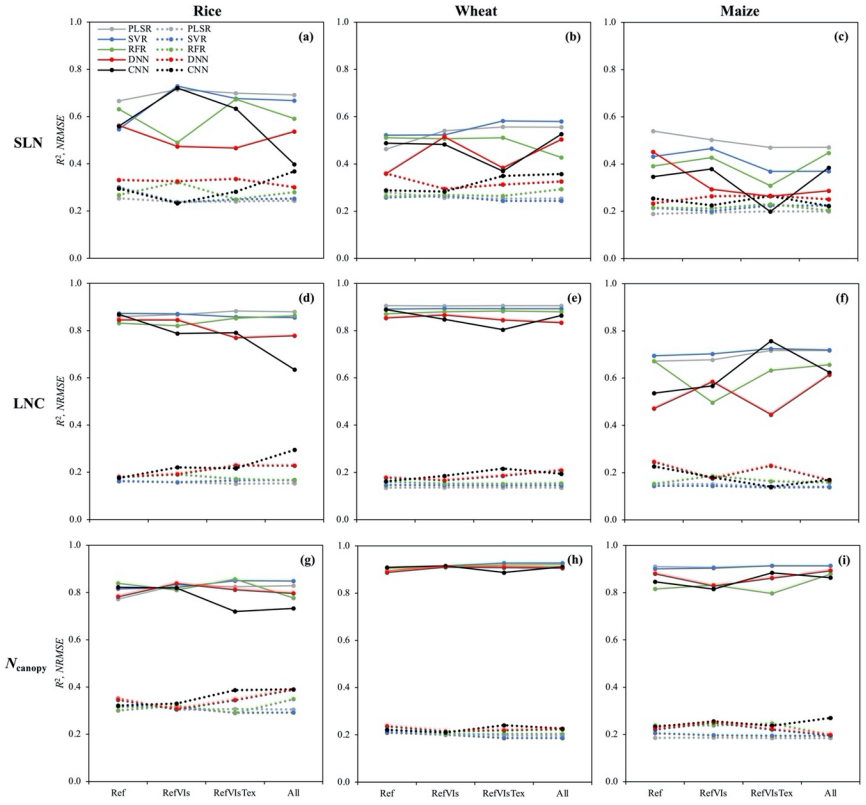

Fig. 4. The prediction performance, R^2 (full lines) and *NRMSE* (dotted lines), in the testing dataset of different regression models in directly predicted specific leaf nitrogen (SLN) (a-c), leaf nitrogen concentration (LNC) (d-f) and canopy nitrogen content (N_{canopy}) (g-i) in rice, wheat and maize with various sets of input feature types. Nonparametric regression algorithms: PLSR = Partial Least Squares Regression, SVR = Support Vector Regression, RFR = Random Forest Regression, DNN = Deep Neural Network, CNN = Convolution Neural Network. Acronyms in the x-axis for four sets of feature types are defined in Table 3.

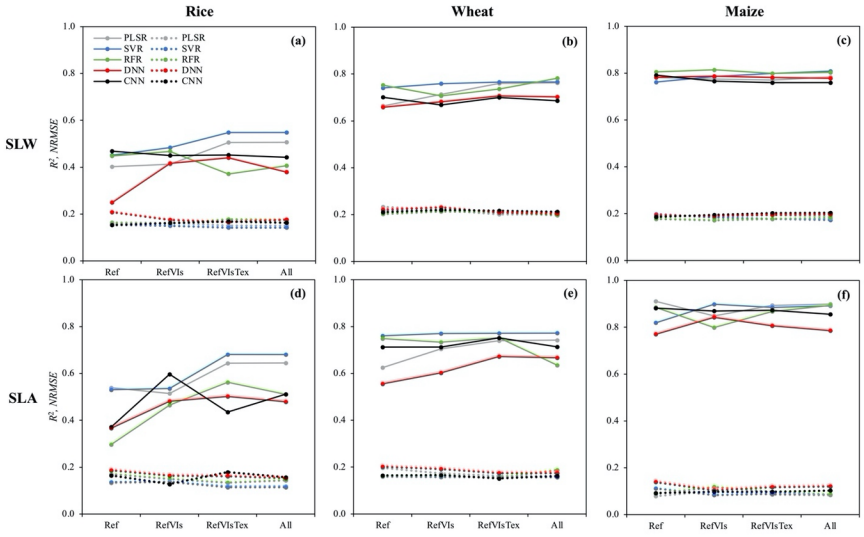

Fig. 5. The prediction performance, R^2 (full lines) and *NRMSE* (dotted lines), in the testing dataset of different regression models in directly predicted specific leaf weight (SLW) (a-c) and specific leaf area (SLA) (d-f) in rice, wheat and maize with various sets of input feature types. Nonparametric regression algorithms: PLSR = Partial Least Squares Regression, SVR = Support Vector Regression, RFR = Random Forest Regression, DNN = Deep Neural Network, CNN = Convolution Neural Network. Acronyms in the x-axis for four sets of feature types are defined in Table 3.

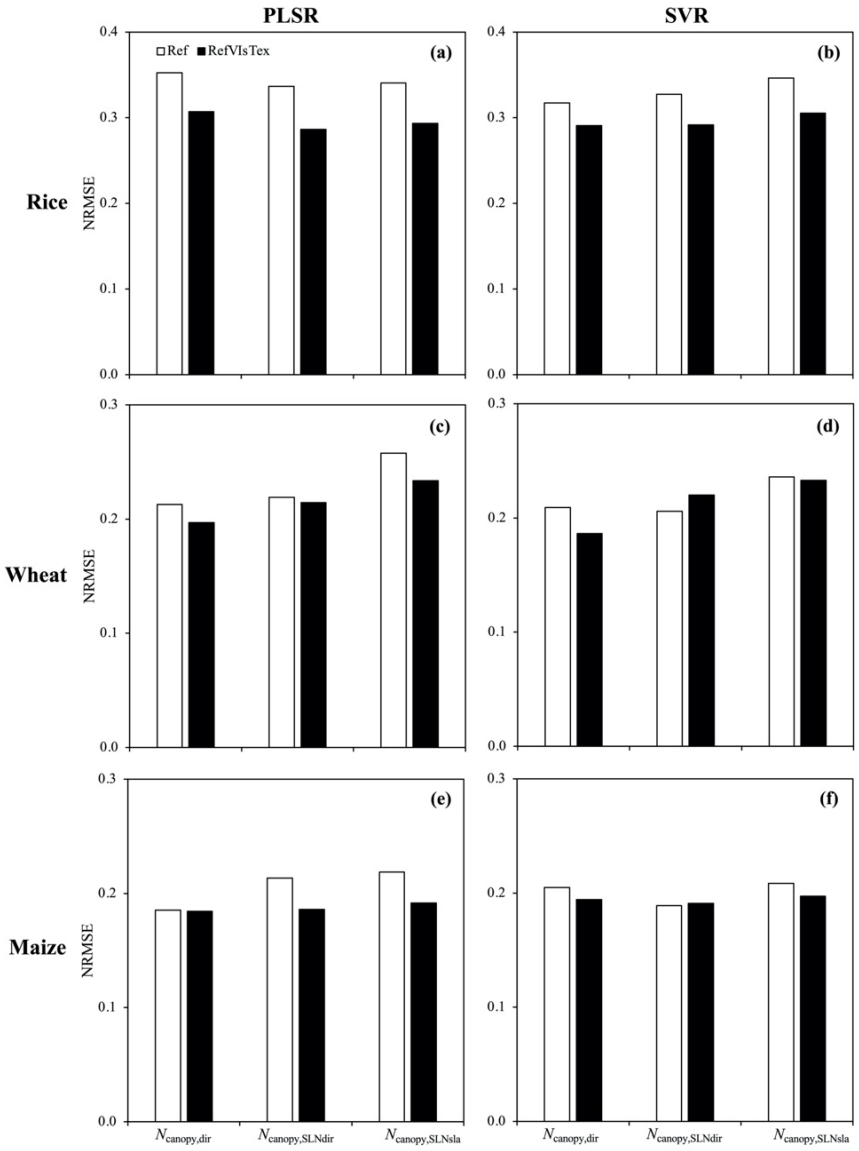

Fig. 6. The prediction performance in the testing dataset of directly and indirectly predicted canopy nitrogen content (N_{canopy}) in rice (a, b), wheat (c, d) and maize (e, f) using feature sets of Ref and RefVIsTex (see Table 3 for their definition) and regression algorithms of Partial Least Squares Regression (PLSR) and Support Vector Regression (SVR). The directly predicted N_{canopy} was labeled as $N_{canopy,dir}$. The indirectly predicted $N_{canopy,SLNdir}$ and $N_{canopy,SLNsla}$ were upscaled from directly predicted specific leaf nitrogen (SLN) SLN_{dir} and from indirectly predicted SLN_{sla}, respectively (also see Table 1).

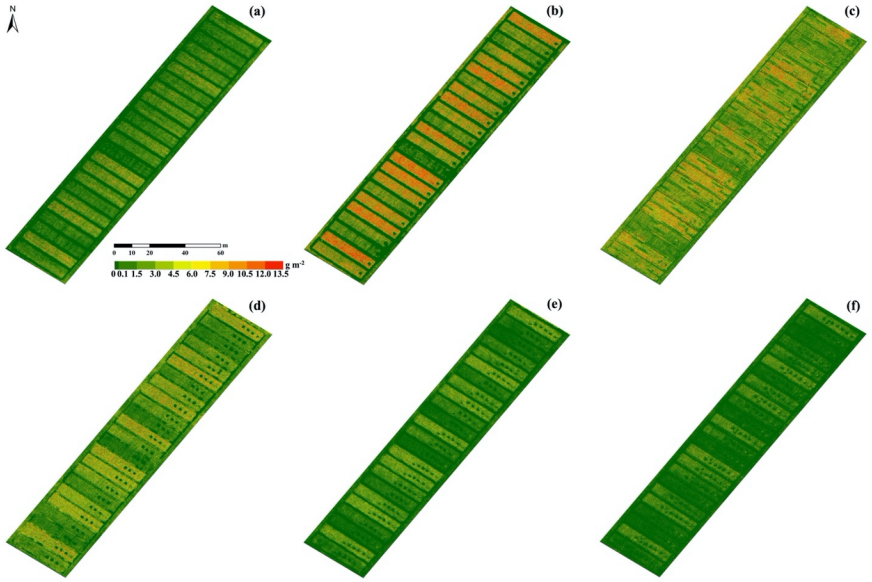

Fig. 7. The predicted canopy nitrogen content (N_{canopy}) from its indirect predictions$N_{\text{canopy,SLNdir}}$ (see Table 1 for its definition) at the experimental area of rice across the whole growing season using feature set of RefVIsTex (see Table 3 for its definition) and regression algorithm of Partial Least Squares Regression. Predicted$N_{\text{canopy,SLNdir}}$ at the stage of tillering (a), stem-elongating (b), flowering (c), ca. 15 days after flowering (d), ca. 30 days after flowering (e), and maturity (f) are shown.